





Droop K -Sharing Function for Energy Management of DC Microgrids

Guilherme Henrique Favaro Fuzato , *Member, IEEE*, Cassius Rossi de Aguiar , Thales Augusto Fagundes ,
Wagner Coelho Leal, Juan C. Vasquez , *Senior Member, IEEE*, Josep M. Guerrero , *Fellow, IEEE*,
and Ricardo Quadros Machado , *Senior Member, IEEE*

Abstract—Slow dynamic response sources, such as fuel cells, are frequently used with faster units, such as batteries and ultracapacitors. In this context, this article gathers the advantages of two energy management techniques to propose the droop k -sharing function. In droop control, energy management is easily implemented using the virtual resistances concept, eliminating the need for fast communication links between the sources. The k -sharing function improves the performance of microgrids with slower sources assigning a preestablished dynamic behavior using a low-pass filter, while the storage unit absorbs the fast transients. Additionally, the k -sharing function also enables the storage unit to share power at a steady state. Therefore, the main advantage of the proposed energy management algorithm is that the control loops of each power source are not coupled to each other, which is accomplished by designing the k -sharing function similarly to the droop technique, eliminating the need for high-speed links of communication and improving the microgrid speed response during fast changes of load. The effectiveness of the proposed function and the theoretical analysis are evaluated using a dc microgrid composed of an H-1000 fuel cell manufactured by Horizon Fuel Cells and three Zippy Compact 5000 25 C Li-Ion batteries in series connection.

Index Terms—Batteries, dc–dc power conversion, energy management, fuel cells.

I. INTRODUCTION

IN DC microgrids, the ability to suppress the effects of load variations is related to the dynamic response of the power

sources connected to the dc-link. If the dynamic response of the sources does not match with the dynamic response of the loads, the microgrid may exhibit undesirable power quality behaviors, such as long-term voltage dips and voltage fluctuations. In this context, several algorithms suggest the use of batteries or ultracapacitors to mitigate the slow dynamic response of sources such as fuel cells [1]–[5].

In fuel cells, when a step of load is applied, the sudden current increase can activate the system protection due to the low voltage cell, if the drained oxygen or hydrogen cannot be replenished immediately or sufficiently. This phenomenon is referred to as cell starvation and can lead the system to stall, permanent cell damage, or reduce the cell lifetime [6], [7].

Another important aspect in microgrids is to determine how much power each source delivers to the dc-link as the power demanded by the load changes. In this context, according to [8], the energy management algorithms can be divided into two main branches: methods based on droop methods and active current sharing (ACS) methods. The droop methods can be easily implemented by using the concept of a virtual negative resistance.

In dc microgrids, the virtual negative resistance establishes a relationship between the dc-link voltage and current injected by each dc–dc converter; hence, as the dc-link voltage drops due to the load connection, the current injected by the dc–dc converter increases. The main disadvantage of this method is that the dc-link voltage exhibits a poor regulation, on the other hand, this feature eliminates the need for a high-speed link of communication between the dc–dc converters [9], [10]. According to [11], the main ACS methods are the master–slave configuration, common duty-ratio control, current control, sensorless current control, and cross-feedback control. In the master–slave configuration, the master dc–dc converter controls the dc-link voltage, while the other converters try to synchronize their currents with the master converter [12].

In the duty-ratio control, the same duty-cycle is applied to all dc–dc converter modules [13]; however, it should be noted that the current sharing of the input current or the load current cannot be achieved with accuracy, due to the differences of the individual modules. Higher accuracy in the current shared between the dc–dc converter modules is accomplished in the current control methods by using techniques such as peak current mode control, charge current mode control, and average current mode control [14], [15]. In the sensorless current control

Manuscript received May 23, 2020; revised November 3, 2020; accepted February 10, 2021. Date of publication April 21, 2021; date of current version June 18, 2021. This work was supported in part by the Coordination for the Improvement of Higher Education Personnel (CAPES) under Grants PDSE-88881.187771/2018-01 and 88881.030370/2013-0 and in part by the São Paulo Research Foundation (FAPESP) under Grants 2013/20721-4 and 2020/05865-3. (Corresponding author: Guilherme Henrique Favaro Fuzato.)

Guilherme Henrique Favaro Fuzato is with the Federal Institute of Education, Science and Technology of São Paulo, Campinas 13059-581, Brazil (e-mail: guilherme.fuzato@gmail.com).

Cassius Rossi de Aguiar is with the Computer Engineering Department, The Federal University of Technology, Toledo 85902-490, Brazil (e-mail: cassiusaguaiar@utfpr.edu.br).

Thales Augusto Fagundes, Wagner Coelho Leal, and Ricardo Quadros Machado are with the Electrical Engineering and Computer Department of the São Carlos School of Engineering, University of São Paulo, São Carlos 13566-590, Brazil (e-mail: fagundes.thales@gmail.com; wagnercoelhoal@gmail.com; rquadros@sc.usp.br).

Juan C. Vasquez and Josep M. Guerrero are with the Department of Energy Technology, University of Aalborg, 9220 Aalborg, Denmark (e-mail: juq@et.aau.dk; joz@et.aau.dk).

Color versions of one or more figures in this article are available at <https://doi.org/10.1109/JESTIE.2021.3074889>.

Digital Object Identifier 10.1109/JESTIE.2021.3074889

presented in [16], a constant duty-cycle perturbation is used to estimate the parameter mismatch between the modules. The mismatch estimation is used to calculate the required duty-cycle compensation to equalize the output current. Besides, in the cross-feedback control [17], the current of each module is used in the control loop of the other modules to generate the duty-cycle of each module.

Finally, in [4], the k -sharing function is implemented using an ACS method by controlling the dc-link voltage using a constant voltage reference and a proportional-integral (PI) voltage controller. An important feature of this function is the ability to suppress fast transients in microgrids with slow dynamic sources, such as fuel cells, using fast dynamic storage devices. Despite of using a PI controller in the dc voltage control loop, which requires a high-speed communication link between the two sources, the k -sharing function, implemented in [4] still produced a small steady-state deviation of the dc-link voltage (1.4%), which depends on the adjustment of the k -sharing function parameters. Additionally, in [4], the k -sharing function only allows the storage devices to inject power in the steady state in the microgrid if the fuel cell reached the maximum power.

A common aspect of the ACS control methods is that the control structures for all dc–dc converters are implemented in the same processor or it is used a high-speed link of communication between the modules to implement the control loops. In this context, there is a lack of techniques in the literature that are designed to mitigate the fast transients of load in microgrids with slow sources, such as fuel cells, without the need to implement the control loops in a single processor or to use high-speed communication links between the power sources. Therefore, in this article, it is proposed the droop k -sharing technique. This technique was designed by gathering the best features of the k -sharing function proposed in [4] with the droop technique.

The main advantage of the droop k -sharing technique is that the storage device can be designed to absorb the transients and share power at the steady state with the other sources in the microgrid without the need for a high-speed link of communication between them. Besides increasing the microgrid maximum available power, the ability to share power at the steady state improves the flexibility for designing energy management algorithms in higher hierarchical levels, where it can be considered other variables such as, the hydrogen cost, fuel cell warm up, State of Charge of the batteries and additional variables with the inclusion of more sources in the microgrid (charging batteries using photovoltaic modules, for example).

Additionally, in [4], the k -sharing function is designed in a more complex way, because the gain (k_{ps}) must be adjusted to mitigate the dc-link voltage steady-state error and to improve the speed response of the k -sharing function. In the droop k -sharing technique, the k -sharing function (k_s) is designed as simple as the droop controller. In this context, the design of the droop controllers and k_s function can also be accomplished using a graphical approach, as usually performed for droop controllers. Since the droop k -sharing technique is a nonlinear control technique, besides the fact that all dc–dc converters have a nonlinear behavior, it is important to evaluate the stability of the microgrid

considering the interaction of the dc–dc converter modules with the designed control structures.

This article is organized as follows. In Section II, the droop k -sharing concept is introduced, while Section III describes the physical structure and the control scheme. In Section IV, the closed-loop of each power source is analyzed to produce the full closed-loop microgrid model presented in Section V. To validate the effectiveness of the proposed solution, in Section VI, we accomplish the analysis of stability and compare the simulations with a set of experimental results. Finally, Section VII concludes this article.

II. DROOP K -SHARING

The fuel cell slow dynamic response is related, mainly, to the cell starvation, but is also associated with the double charge effect and to the time that the reaction takes to reach a new equilibrium state [6], [7], [18]. Since this phenomenon presents a nonlinear behavior and depends on other physical variables, such as temperature, membrane humidity, and others, it is difficult to model the dynamic response with a high accuracy.

With these arguments in mind, a common strategy among the control methods for fuel cells consists of associating a preestablished dynamic response to the fuel cell using a low-pass filter. The time constant of this filter is designed to operate with a cutoff frequency lower than the fuel cell time response. To mitigate the negative effects on the microgrid stability of this low-pass filter, as well as the inherent slow response of the fuel cell, it is used as a storage system capable to deliver power at a higher speed [1]–[4]. For this purpose, in this article, a Li-Ion battery stack is used.

Considering the arguments presented in the previous paragraphs, in the fuel cell control structure, the droop reference $i_{\text{droop_fc}}$ is associated with a first-order low-pass filter $n_d(s)$ with a preestablished time constant τ

$$n_d(s) = \frac{1}{s\tau + 1}. \quad (1)$$

Since the goal is to associate a preestablished dynamic response to the fuel cell, a first-order low-pass filter is chosen to minimize the computational cost in the experimental implementation. With the inclusion of this filter, the current reference $i_{\text{ref_fc}}$ slowly moves to the steady-state value of $i_{\text{droop_fc}}$ ($I_{\text{droop_fc}}$) after a step of load is applied on the dc-link:

$$i_{\text{ref_fc}}(s) = i_{\text{droop_fc}}(s)n_d(s). \quad (2)$$

Therefore, using the final value theorem, the fuel cell current reference at the steady state ($I_{\text{ref_fc}}$) is defined by

$$I_{\text{ref_fc}} = \lim_{s \rightarrow 0} I_{\text{droop_fc}} \frac{s}{s} \frac{1}{s\tau + 1} = I_{\text{droop_fc}}. \quad (3)$$

To ensure the stability of the dc microgrid, the complementary frequency spectrum is assigned to the battery stack ($1 - n_d(s)$). In this case, during a step of load, the fuel cell ($i_{\text{in_fc}}$) and battery ($i_{\text{in_bat}}$) terminal currents, which are the input currents of the dc–dc converters, would present the behavior illustrated in Fig. 1(a). In this figure, the battery absorbs the high-frequency

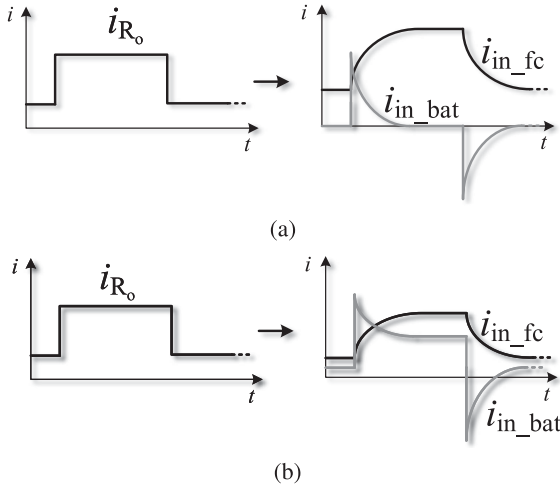


Fig. 1. Fuel cell and battery currents with a load step using the k -sharing function (a) $k_s = 1$. (b) $0 \leq k_s < 1$.

spectrum transients during the load steps (i_{R_o}), but the steady-state current is null, because, applying the final value theorem in i_{ref_bat} , the steady-state current reference I_{ref_bat} is null:

$$\begin{aligned} I_{ref_bat} &= \lim_{s \rightarrow 0} I_{droop_fc} \frac{s}{s} \left(1 - \frac{1}{s\tau + 1} \right) \\ &= I_{droop_fc} (1 - 1) = 0 \end{aligned} \quad (4)$$

where I_{droop_fc} represents the steady-state droop current reference.

With the aim to make the battery stack able to inject power at the steady state, the k -sharing function (k_s) is added in the battery control structure. According to [4], the k -sharing function works as an adaptive function, which changes according to the dc-link voltage value. This algorithm is introduced in the battery control scheme by multiplying the k -sharing function to the $n_d(s)$ filter:

$$i_{ref_bat}(s) = i_{droop_fc}(s) [1 - k_s n_d(s)]. \quad (5)$$

With the inclusion of the k -sharing function, the steady-state current reference for the battery (I_{ref_bat}) is

$$\begin{aligned} I_{ref_bat} &= \lim_{s \rightarrow 0} I_{droop_fc} \frac{s}{s} \left(1 - \frac{k_s}{s\tau + 1} \right) \\ &= I_{droop_fc} (1 - k_s). \end{aligned} \quad (6)$$

Considering the result of (6), for the k -sharing function in the interval of $1 \geq k_s \geq 0$, the battery current reference at the steady state would be between $0 \leq I_{ref_bat} \leq I_{droop_fc}$. Consequently, as illustrated in Fig. 1(b), with the k -sharing function, the battery not only absorbs the high-frequency spectrum during the transients, but also share the power injected at the steady state with the fuel cell.

It is important to notice that a relevant feature of this method is that the control loops of the battery and fuel cell are not coupled with each other, the only link between the two systems is the dc-link voltage. Also, the k -sharing function can be designed

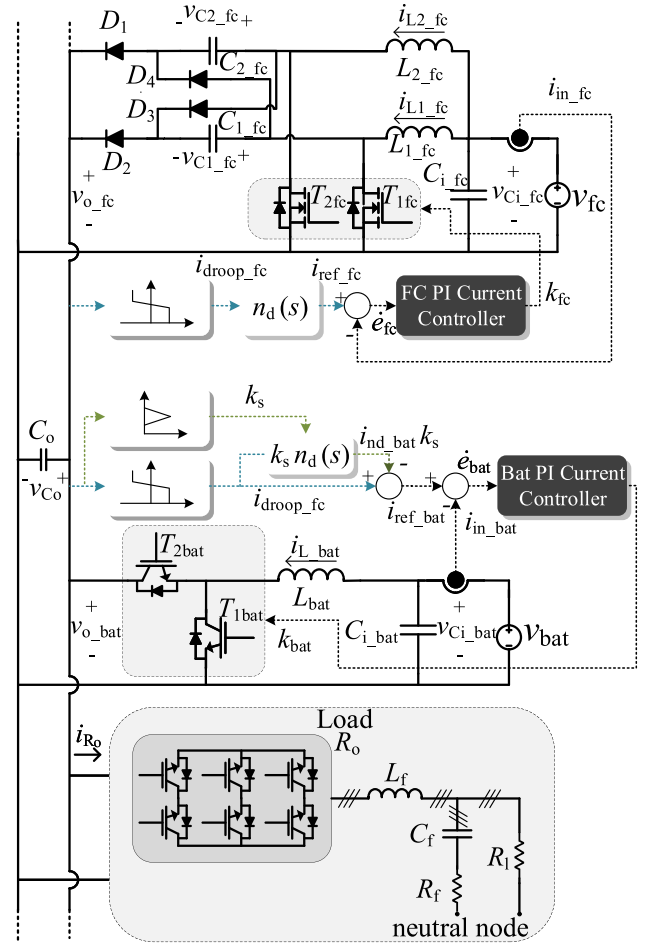


Fig. 2. Microgrid scheme.

as simple as a droop algorithm, since k -sharing function also depends on the dc-link voltage.

III. SYSTEM DESCRIPTION

The dc microgrid used to validate the control algorithm and stability analysis proposed in this article is presented in Fig. 2. In this figure, each source is connected to the dc-link using a dc-dc converter, while a three-phase inverter in islanded operation is used as load connected to the dc-link.

Each source requires a dc-dc converter structure designed considering the input voltage and current characteristics. For the Li-Ion battery with a v_{bat} terminal voltage, it is used a buck-boost bidirectional converter. This converter has a input capacitor C_{i_bat} with voltage v_{Ci_bat} and a inductor L_{bat} that is connected to a pair of IGBTs (T_{1bat} and T_{2bat}). The transistors are switched using a synchronous modulation, i.e., when T_{1bat} is closed, T_{2bat} is open; when T_{1bat} is open, T_{2bat} is closed. In this case, the direction of the current i_{L_bat} depends mainly on the input voltage (v_{bat}), output voltage (v_{o_bat}), and duty-cycle (k_{bat}).

For the fuel cell, with a terminal voltage of v_{fc} , as mentioned in [19], it is recommended to use a dc-dc converter with a high voltage gain and able to process a high input current. Therefore,

it is used an interleaved boost with voltage multiplier (IBVM) converter, which consists of an interleaved boost converter with two phases switched 180° apart from each other, with a voltage multiplier cell connected in series. The source is connected to the input capacitor C_{i_fc} with voltage v_{Ci_fc} and inductors of the two phases L_{1_fc} , L_{2_fc} with current i_{L1_fc} , i_{L2_fc} . To achieve a higher voltage gain, the MOSFETs (T_{1fc} and T_{2fc}) are switched with a duty-cycle above 50%. In series with the boost interleaved structure, it is connected a voltage doubler with four diodes (D_1 , D_2 , D_3 , and D_4) and two capacitors (C_{1_fc} and C_{2_fc}) with voltages v_{C1_fc} and v_{C2_fc} .

The dc-link, where the dc-dc converters and inverter are connected, has an equivalent capacitance C_o with a voltage v_{Co} . The three-phase bridge inverter used as load is implemented using an LC filter (L_f , C_f , and R_f) with a local ac resistive load R_l that is switched using steps of load. In the dynamic model, the inverter is modeled as a dc resistance R_o with a dc current i_{Ro} .

Regarding the control structure, in both dc-dc converters, the inner loop controls the input current while the outer loop is responsible for the energy management control strategy. In the fuel cell control structure, the inner loop is implemented by measuring the input current i_{in_fc} and comparing it with the current reference i_{ref_fc} . The error (\dot{e}_{fc}) is used as input of the fuel cell PI controller, which generates the duty-cycle k_{fc} for the pair of MOSFETs. In the outer loop, the dc-link voltage ($v_{o_fc} = v_{Co}$) is the input of the droop controller. Finally, the current reference (i_{ref_fc}) is generated by using the low-pass filter $n_d(s)$ in the droop controller output current i_{droop_fc} , as shown in (2).

For the battery control structure, the inner loop is implemented identically to the fuel cell current control loop. The battery input current i_{in_bat} is measured and compared with the current reference i_{ref_bat} , which generates the error \dot{e}_{bat} that is used in the PI controller to switch the IGBTs with a duty-cycle k_{bat} . In the outer loop, the dc-link voltage ($v_{o_bat} = v_{Co}$) is measured and used in the droop controller to generate the droop reference i_{droop_fc} . As presented in (5), the battery current control loop is designed for the complementary spectrum of frequency; therefore, the variable i_{droop_fc} is subtracted by $i_{droop_fc}n_d(s)k_s = i_{nd_bat}k_s$ to generate the current reference i_{ref_bat} . The k -sharing function k_s is included in the outer control loop as an adaptive gain by measuring the dc-link voltage.

IV. CLOSED-LOOP MODEL

In this section, the fuel cell and the storage systems are modeled considering the closed-loop equations. In both cases, there are two main control loops, the inner control loop regulates the input current, while the outer loop is associated with the energy management strategy. The energy management strategy is accomplished using the droop technique and the droop k -sharing function, which uses the dc-link voltage measurement. Besides, the difference between the fuel cell and battery control schemes are associated with the k -sharing function, i.e., the fuel cell is designed to absorb the slow part of the transients, while the battery absorbs the fast part of the transients.

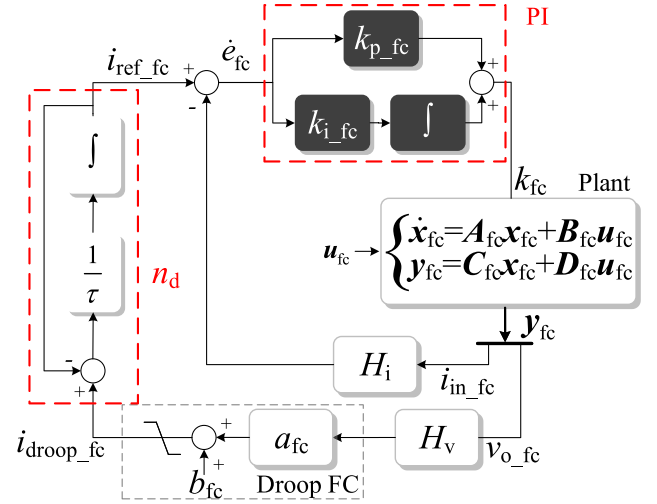


Fig. 3. Fuel cell control scheme.

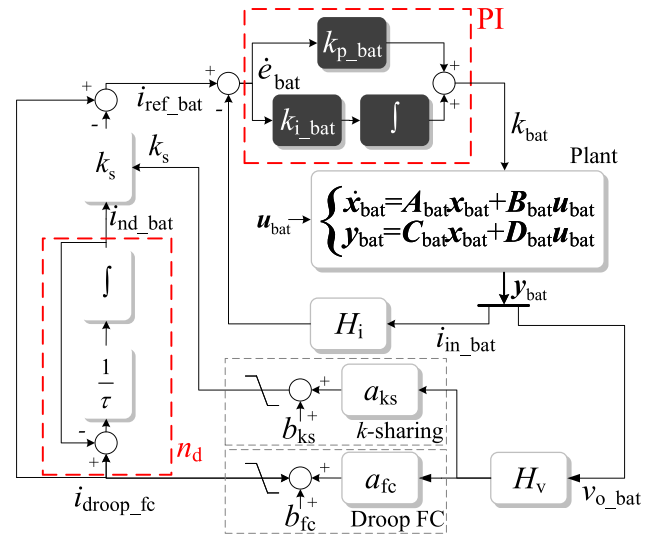


Fig. 4. Battery control scheme.

A. Fuel Cell Closed-Loop Model

Fig. 3 presents the fuel cell control scheme. In this control structure, the plant is the average model IBVM converter (7), which was modeled and analyzed in [19]–[21]. The model (7) derives from the generic state-space average model presented in Appendix A.

According to Fig. 3 and (7), the manipulated variable for the IBVM converter average model is the duty-cycle k_{fc} , while the output vector (y) contains the IBVM input current (i_{in_fc}) and the output voltage (v_{o_fc}). Equation (7) is shown at bottom of the next page, where the state-space variables are defined as follows: $x_{fc} = [v_{Ci_fc} \ i_{L1_fc} \ i_{L2_fc} \ v_{C1_fc} \ v_{C2_fc} \ v_{Co_fc}]^T$, $u_{fc} = v_{fc}$, $A_{fc0} = 2A_{fc1} - A_{fc2} - A_{fc4}$, and $A_{fc0} = -A_{fc1} + A_{fc2} + A_{fc4}$, considering that $A_{fc1} = A_{fc3}$, $A_{fc2} = A_{fc3}$, A_{fc4} are the state matrices for each switching interval, i.e., T_{1fc} and T_{2fc} closed (A_{fc1}), T_{1fc} open and T_{2fc} closed (A_{fc2}), T_{1fc} and T_{2fc} closed (A_{fc3}), T_{1fc} closed and T_{2fc} open (A_{fc4}),

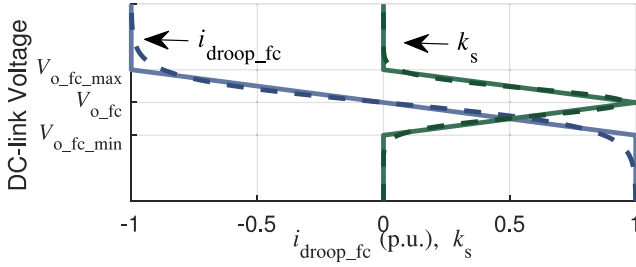


Fig. 5. Droop controller and k -sharing curves for the management control loop.

respectively. These equations are also applied to the matrices B_{fc} , C_{fc} , and D_{fc} .

The dc-dc converter input current is measured using a sensor of gain H_i and compared with the reference i_{ref_fc} generated by the outer loop. The error \dot{e}_{fc} is used as input of the PI controller with a proportional gain k_{p_fc} and integral gain k_{i_fc} . In the outer loop, the output voltage is measured by a sensor of gain H_v . The measurement signal is used in the droop controller shown in Fig. 3, which corresponds to (8) saturated in the fuel cell maximum current. As mentioned in Section II, the fuel cell control loop is designed to absorb the current low frequencies during transients; therefore, the current reference i_{ref_fc} is generated from the droop controller output using a low-pass filter $n_d(s)$

$$i_{droop_fc} = \begin{cases} -1, & V_{o_fc_max} < v_{o_fc} \\ a_{fc}v_{o_fc}H_v + b_{fc}, & V_{o_fc_min} < v_{o_fc} \leq V_{o_fc_max} \\ 1, & v_{o_fc} \leq V_{o_fc_min} \end{cases} \quad (8)$$

where the coefficients are defined as $a_{fc} = \frac{1}{V_{o_fc_min} - V_{o_fc_0}}$ and $b_{fc} = \frac{V_{o_fc_0}}{V_{o_fc_min} - V_{o_fc_0}}$ with $H_v = 1$.

The fuel cell droop controller $i_{droop_fc} = a_{fc}v_{o_fc}H_v + b_{fc}$ is represented by the continuous blue line in Fig. 5. Although the fuel cell is an unidirectional source, the per-unit (p.u.) current reference is in the range of -1.0 p.u. ($V_{o_fc_max}$) to 1.0 p.u. ($V_{o_fc_min}$), with 0.0 p.u. in $V_{o_fc_0}$. Since the droop controller i_{droop_fc} is the same for the battery and the fuel cell, the negative part of i_{droop_fc} is only used in the battery control loop. Therefore, the fuel cell does not inject current in the point of common coupling if the dc-link voltage is higher than $V_{o_fc_0}$ (zero droop current reference), while the maximum current drawn from the fuel cell occurs for dc-link voltages lower than $V_{o_fc_min}$.

To apply the Lyapunov's indirect method in the stability analysis, the microgrid model must be continuously differentiable. However, the droop controller is abruptly limited from -1.0

to 1.0 p.u., which is in fact the composition of three different functions, one for voltages higher than $V_{o_fc_max}$, one for voltages lower than $V_{o_fc_min}$, and one function for voltages between $V_{o_fc_min}$ and $V_{o_fc_max}$. Hence, the droop controller is approximated by the sigmoid function (9), which is represented by the dashed blue line in Fig. 5, where the slope of the curve is mostly associated with the constant α_{fc} and the curve translation is related with $V_{o_fc_0}$

$$i_{droop_fc} = 1 - \frac{2}{1 + e^{-\alpha_{fc}(v_{o_fc}H_v - V_{o_fc_0})}}. \quad (9)$$

As the plant and controllers are now continuously differentiable, using the control scheme presented in Fig. 3, the plant model (7), and the droop controller sigmoid approximation (9), the closed-loop model (10) is obtained. In this model, there is a differential equation for the physical storage components (inductors and capacitors) and the control loop storage elements (integrators). The first line of (10) is associated with the IBVM storage components, which is obtained from the (7) state variables (\dot{x}_{fc}). The second line of (10) is related to the integrator in the PI controller, and it is obtained by equating the error variable in the current control loop (\dot{e}_{fc}). Finally, the last line of (10) derives from the filter $n_d(s)$. Since the droop controller is designed using a per-unit reference (i_{droop_fc}), in i_{ref_fc} equation, the droop reference is multiplied by the fuel cell maximum current I_{fc_max}

$$\begin{cases} \dot{x}_{fc} = (A_{fc0} + k_{fc}A_{fck})x_{fc} + (B_{fc0} + k_{fc}B_{fck})u_{fc} \\ \dot{e}_{fc} = i_{ref_fc} - H_i i_{in_fc} \\ i_{ref_fc} = \frac{1}{\tau} [I_{fc_max} i_{droop_fc} - i_{ref_fc}] \end{cases} \quad (10)$$

where $k_{fc} = k_{p_fc}\dot{e}_{fc} + k_{i_fc}e_{fc}$ is the IBVM duty-cycle.

B. Storage Closed-Loop Model

In contrast to the fuel cell control scheme, in the battery control scheme presented in Fig. 4, the k -sharing function (k_s) is associated with the droop controller to control the amount of power injected by the battery in the point of common coupling during the steady state.

In a similar way to the fuel cell control scheme, the inner loop in Fig. 4 is responsible to control the input current of the buck-boost bidirectional converter. For this purpose, the battery current i_{in_bat} is measured using a sensor of gain H_i and compared with the current reference i_{ref_bat} . The error generated by this comparison \dot{e}_{bat} is used as input of the PI controller with a proportional gain k_{p_bat} and an integral gain k_{i_bat} . The output of the PI controller is defined as the duty-cycle of the battery dc-dc converter k_{bat} , which is the input of the average bidirectional buck-boost converter model, represented

$$\begin{cases} \dot{x}_{fc} = (\underbrace{A_{fc0} + k_{fc}A_{fck}}_{A_{fc}})x_{fc} + (\underbrace{B_{fc0} + k_{fc}B_{fck}}_{B_{fc}})u_{fc} \\ y_{fc} = \begin{bmatrix} i_{in_fc} \\ v_{o_fc} \end{bmatrix} = \underbrace{\begin{bmatrix} C_{fc0i} + k_{fc}C_{fcki} \\ C_{fc0v} + k_{fc}C_{fckv} \end{bmatrix}}_{C_{fc}}x_{fc} + \underbrace{\begin{bmatrix} D_{fc0i} + k_{fc}D_{fcki} \\ D_{fc0v} + k_{fc}D_{fckv} \end{bmatrix}}_{D_{fc}}u_{fc} \end{cases} \quad (7)$$

by the nonlinear state-space model (11). The model (11) also derives from the generic state-space average model presented in Appendix A. Equation (11) is shown at the bottom of this page, where $\mathbf{x}_{\text{bat}} = [v_{\text{Ci_bat}} \ i_{\text{L_bat}} \ v_{\text{Co_bat}}]^T$, $\mathbf{u}_{\text{bat}} = v_{\text{bat}}$, $\mathbf{A}_{\text{batk}} = \mathbf{A}_{\text{bat1}} - \mathbf{A}_{\text{bat2}}$, and $\mathbf{A}_{\text{bat0}} = \mathbf{A}_{\text{bat2}}$, considering that \mathbf{A}_{bat1} and \mathbf{A}_{bat2} are the state matrices for the switching interval where $T_{1\text{bat}}$ is closed and $T_{2\text{bat}}$ is open, $T_{1\text{bat}}$ is open and $T_{2\text{bat}}$ is closed, respectively. This modeling process is also applied to the average matrices \mathbf{B}_{bat} , \mathbf{C}_{bat} , and \mathbf{D}_{bat} .

The energy management strategy for the battery, also implemented in the outer control loop, is performed by measuring the dc-dc converter output voltage $v_{\text{o_bat}}$ with a sensor of gain H_v and using this signal as input of the k -sharing and droop controllers. The droop controller is the same as used for the fuel cell, with the exception that, in this case, the droop current per-unit reference ($i_{\text{droop_fc}}$) is multiplied by the battery maximum current $I_{\text{bat_max}}$.

Both curves, k -sharing and droop are presented in Fig. 5. The k -sharing curve, in continuous green line, derives from the following set of linear equations limited at $1 \geq k_s \geq 0$:

$$k_s = \begin{cases} 0, & V_{\text{o_fc_max}} < v_{\text{o_bat}} \\ -v_{\text{o_bat}} H_v a_{ks} + b_{ks2}, & V_{\text{o_fc_0}} < v_{\text{o_bat}} \leq V_{\text{o_fc_max}} \\ v_{\text{o_bat}} H_v a_{ks} + b_{ks1}, & V_{\text{o_fc_min}} < v_{\text{o_bat}} \leq V_{\text{o_fc_0}} \\ 0, & v_{\text{o_bat}} \leq V_{\text{o_fc_min}} \end{cases} \quad (12)$$

where $V_{\text{o_fc_min}}$, $V_{\text{o_fc_max}}$, and $V_{\text{o_fc_0}}$ are constant values defined by the designer and are associated with the minimum, maximum, and middle dc-link voltage, respectively. Also, the coefficients are defined by $a_{ks} = \frac{1}{V_{\text{o_fc_0}} - V_{\text{o_fc_min}}}$, $b_{ks1} = \frac{V_{\text{o_fc_min}}}{V_{\text{o_fc_min}} - V_{\text{o_fc_0}}}$, and $b_{ks2} = \frac{V_{\text{o_fc_max}}}{V_{\text{o_fc_0}} - V_{\text{o_fc_min}}}$ with $H_v = 1$.

The continuously differentiable approximation for k_s function is performed using the sigmoid function as follows

$$k_s = \beta_{ks1} e^{-\left[\frac{(H_v v_{\text{o_bat}} - V_{\text{o_fc_0}})^2}{\beta_{ks2}}\right]} \quad (13)$$

where β_{ks1} defines the maximum value of k_s , β_{ks2} defines the slope of the k -sharing curve, and $V_{\text{o_fc_0}}$ is associated with the translation of the sigmoid function.

The microgrid operation, based on the designed curves presented in Fig. 5, can be described considering four different layers of operation. First, the dc-link voltage is above $V_{\text{o_fc_max}}$ and the microgrid absorbs the excess of power in the dc-link. According to (6), in this layer, the battery absorbs the maximum current $I_{\text{ref_bat}} = -1(1 - 0) = -1$ p.u., while the fuel cell current at the steady state is null. In the second layer, if the dc-link voltage drops to a voltage higher than $V_{\text{o_fc_0}}$ and lower than $V_{\text{o_fc_max}}$, the fuel cell current remains null, while the current

absorbed by the battery increases from $I_{\text{ref_bat}} = -1$ p.u. in $V_{\text{o_fc_max}}$ to $I_{\text{ref_bat}} = -1(1 - 1) = 0$ p.u. in $V_{\text{o_fc_0}}$.

In the third layer, as the load connected in the dc-link increases, the dc-link voltages drops below $V_{\text{o_fc_0}}$. In this case, using (3), the fuel cell starts injecting power in the dc-link with input current reference that goes from $I_{\text{ref_fc}} = 0$ p.u. in $V_{\text{o_fc_0}}$ to $I_{\text{ref_fc}} = 1$ p.u. in $V_{\text{o_fc_min}}$, while the battery shares the injected power with a current reference of $I_{\text{ref_bat}} = 0$ p.u. to $I_{\text{ref_bat}} = 1(1 - 0) = 1$ p.u. In the last layer, the dc-link voltage drops below $V_{\text{o_fc_min}}$; therefore, both sources try to inject the maximum current to avoid the dc-link collapse by using the references $I_{\text{ref_fc}} = 1$ p.u. and $I_{\text{ref_bat}} = 1$ p.u.

Using the dc-dc converter average model (11) and the k_s sigmoid approximation (13), the set of differential equations (14) shown at bottom the next page, that represents the battery closed-loop system, according to Fig. 4, is obtained. The first equation comprehends the dynamic behavior of the storage components in the dc-dc converter circuit ($\dot{\mathbf{x}}_{\text{bat}}$), while the second equation is related to the integrator part of the PI controller (\dot{e}_{bat}), which computes the error used as input of the inner loop controller. The last equation models the dynamic behavior of the $n_d(s)$ filter using the integration variable $i_{\text{nd_bat}}$, where $k_{\text{bat}} = k_{p_bat} \dot{e}_{\text{bat}} + k_{i_bat} e_{\text{bat}}$ is the duty-cycle of the bidirectional buck-boost converter.

V. FULL MICROGRID MODEL

In this section, the closed-loop models obtained in Section IV are coupled to obtain a full microgrid model. The models are coupled using the dc-link capacitor differential equation, and, to simplify the coupling process, the parasitic resistances of the output capacitor of both dc-dc converters are not considered. Therefore, it is possible to assume that the dc-link voltage is $v_{\text{Co}} = v_{\text{Co_bat}} = v_{\text{Co_fc}} = v_{\text{o_bat}} = v_{\text{o_fc}}$.

Also, to eliminate the superposition in the dc-link capacitor differential equation during the coupling process, the load term is decreased by $(-\frac{v_{\text{Co}}}{R_{\text{o}} C_{\text{o}}})$, which leads to the full microgrid state-space average nonlinear model (15) shown at bottom of the next page, with fuel cell and battery connected to the dc-link using a IBVM and bidirectional buck-boost, respectively.

VI. RESULTS

This section presents the simulation and experimental results using a dc microgrid composed by a fuel cell and battery. The fuel cell used is the H-1000 by the manufacturer fuel cell Technologies, with 48 cells in series connection, which results in a maximum power of 1 kW (28.8 V; 35 A). Regarding the batteries, three modules of Zippy Compact 5000 25 C in series

$$\begin{cases} \dot{\mathbf{x}}_{\text{bat}} = (\mathbf{A}_{\text{bat0}} + k_{\text{bat}} \mathbf{A}_{\text{batk}}) \mathbf{x}_{\text{bat}} + (\mathbf{B}_{\text{bat0}} + k_{\text{bat}} \mathbf{B}_{\text{batk}}) \mathbf{u}_{\text{bat}} \\ \begin{bmatrix} \dot{i}_{\text{in_bat}} \\ v_{\text{o_bat}} \end{bmatrix} = \underbrace{\begin{bmatrix} \mathbf{C}_{\text{bat0i}} + k_{\text{bat}} \mathbf{C}_{\text{batki}} \\ \mathbf{C}_{\text{bat0v}} + k_{\text{bat}} \mathbf{C}_{\text{batkv}} \end{bmatrix}}_{\mathbf{C}_{\text{bat}}} \mathbf{x}_{\text{bat}} + \underbrace{\begin{bmatrix} \mathbf{D}_{\text{bat0i}} + k_{\text{bat}} \mathbf{D}_{\text{batki}} \\ \mathbf{D}_{\text{bat0v}} + k_{\text{bat}} \mathbf{D}_{\text{batkv}} \end{bmatrix}}_{\mathbf{D}_{\text{bat}}} \mathbf{u}_{\text{bat}} \end{cases} \quad (11)$$

TABLE I
DC-DC CONVERTERS' PARAMETERS

IBVM		Bidirectional Buck-Boost	
Parameters	Values	Parameters	Values
$L_{1_fc} = L_{2_fc}$	870 μ H	L_{bat}	10 mH
$r_{L1_fc} = r_{L2_fc}$	34.8 m Ω	r_{L_bat}	226 m Ω
$C_{1_fc} = C_{2_fc}$	1 μ F	C_{i_bat}	470 μ F
$r_{C1_fc} = r_{C2_fc}$	29 m Ω	r_{Ci_bat}	33 m Ω
$r_{D1} = r_{D2} = r_{D3} = r_{D4}$	53 m Ω	r_{Co_bat}	11 m Ω
$r_{T1fc} = r_{T2fc}$	24 m Ω	r_{i_bat}	50 m Ω
C_{i_fc}	470 μ F	$r_{T1bat} = r_{T2bat}$	0.23 Ω
r_{Ci_fc}	33 m Ω		
r_{Co_fc}	11 m Ω		
r_{i_fc}	5 m Ω		

connection were used. Each module is composed by 6 Li-Ion cells in series connection, resulting in an output voltage of 22.2 V per module.

The simulation results were obtained by solving the microgrid closed-loop model (15) using the ode23tb solver implemented in a MATLAB script. The sources were considered constant at $v_{fc} = 28.8$ V and $v_{bat} = 66.6$ V. Where 28.8 V is the fuel cell voltage at maximum power presented in the datasheet and 66.6 V results from the rated voltage of the series connection of three Li-Ion modules.

For the load in the dc microgrid, it was used as a SEMIKRON inverter module connecting the dc-link to an ac resistive local load. The ac local load is connected to the SEMIKRON module through an LC filter, and the inverter delivers a constant voltage of 63.6 V rms to the load. The LC filter has a 2.0 mH three-phase inductor connected to the inverter terminals. After the inductor, a three-phase capacitor of 10.0 μ F with a series resistance of 10.0 Ω is star-connected in the point where the ac loads are connected.

Table I presents the parameters used for both dc-dc converters, which were obtained by the components used in the experimental setup. This table presents the IBVM converter parasitic resistances of the inductors $r_{L1_fc} = r_{L2_fc}$, voltage multiplier capacitors $r_{C1_fc} = r_{C2_fc}$, diodes of the voltage multiplier cell

TABLE II
CONTROL SCHEME PARAMETERS

Parameters	Values	Parameters	Values
k_{p_fc}	0.0256	$V_{o_fc_min}$	240 V
k_{i_fc}	7.7689	$V_{o_fc_0}$	245 V
k_{p_bat}	0.2916	$V_{o_fc_max}$	250 V
k_{i_bat}	18.227	α_{fc}	0.5391
I_{fc_max}	20.00 A	β_{ks1}	0.9579
I_{bat_max}	5.00 A	β_{ks2}	2.995
$H_v = H_i$	1.00		

$r_{D1} = r_{D2} = r_{D3} = r_{D4}$, transistors $r_{T1fc} = r_{T2fc}$, input capacitor r_{Ci_fc} , output capacitor r_{Co_fc} , and input resistance of the converter r_{i_fc} , according to the model presented in [19] and [21].

The same procedure to obtain the IBVM dynamic model was applied to the buck-boost bidirectional converter; therefore, Table I also includes the parasitic resistances of the inductor r_{L_bat} , input capacitor r_{Ci_bat} , output capacitor r_{Co_bat} , transistors $r_{T1bat} = r_{T2bat}$, and input resistance of the converter r_{i_bat} . Additionally, the total output capacitance, resulted by the connection of the dc-dc converters in the point of common coupling is $C_o = 1360$ μ F, also, the switching frequency used for all the transistors in the experimental setup is 12 kHz.

Table II presents the parameters used in the control scheme. The first four parameters concern the PI current controllers used for both dc-dc converters, which were designed using the procedure described in [21] with phase margins and cutoff frequencies of 87.30° and 1.12 kHz for the fuel cell PI current controller and 74.73° and 1.00 kHz for the battery PI current controller. This table also presents the current limits I_{fc_max} and I_{bat_max} assigned to the fuel cell and battery, respectively. Additionally, Table II also includes the voltages $V_{o_fc_min}$, $V_{o_fc_0}$, and $V_{o_fc_max}$, which are associated with the dc-link voltage range that the droop and k -sharing controllers were designed to operate, as shown in Fig. 5. Finally, the last three parameters in this table are used for the droop and k -sharing curves approximations presented in (9) and (13).

$$\begin{cases} \dot{x}_{bat} = (A_{bat0} + k_{bat}A_{batk})x_{bat} + (A_{bat0} + k_{bat}A_{batk})u_{bat} \\ \dot{e}_{bat} = i_{droop_fc} - i_{nd_bat}k_s - H_i i_{in_bat} \\ \dot{i}_{nd_bat} = \frac{1}{\tau} [I_{bat_max} i_{droop_fc} - i_{nd_bat}] \end{cases} \quad (14)$$

$$\begin{bmatrix} \dot{x}_{fc}^{(1:5)} \\ \dot{e}_{fc} \\ \dot{i}_{ref_fc} \\ \dot{x}_{bat}^{(1:2)} \\ \dot{e}_{bat} \\ \dot{i}_{nd_bat} \\ \dot{v}_{Co} \end{bmatrix} = \begin{bmatrix} \left(A_{fc0}^{(1:5,1:5)} + k_{fc}A_{fck}^{(1:5,1:5)} \right) x_{fc} + \left(B_{fc0}^{(1:5,1:5)} + k_{fc}B_{fck}^{(1:5,1:5)} \right) u_{fc} \\ i_{ref_fc} - H_i i_{in_fc} \\ \frac{1}{\tau} [I_{fc_max} i_{droop_fc} - i_{ref_fc}] \\ \left(A_{bat0}^{(1:2,1:3)} + k_{bat}A_{batk}^{(1:2,1:3)} \right) x_{bat} + \left(B_{bat0}^{(1:2,1:3)} + k_{bat}B_{batk}^{(1:2,1:3)} \right) u_{bat} \\ i_{droop_fc} - i_{nd_bat}k_s - H_i i_{in_bat} \\ \frac{1}{\tau} [I_{bat_max} i_{droop_fc} - i_{nd_bat}] \\ \begin{bmatrix} x_{bat} \\ x_{fc} \end{bmatrix}^T \begin{bmatrix} A_{bat0}^{(3,1:3)} + k_{bat}A_{batk}^{(3,1:3)} \\ A_{fc0}^{(6,1:6)} + k_{fc}A_{fck}^{(6,1:6)} \end{bmatrix} + \dots \\ \dots + \begin{bmatrix} u_{bat} \\ u_{fc} \end{bmatrix}^T \begin{bmatrix} B_{bat0}^{(3,1:3)} + k_{bat}B_{batk}^{(3,1:3)} \\ B_{fc0}^{(6,1:6)} + k_{fc}B_{fck}^{(6,1:6)} \end{bmatrix} - \left(-\frac{v_{Co}}{R_o C_o} \right) \end{bmatrix} \quad (15)$$

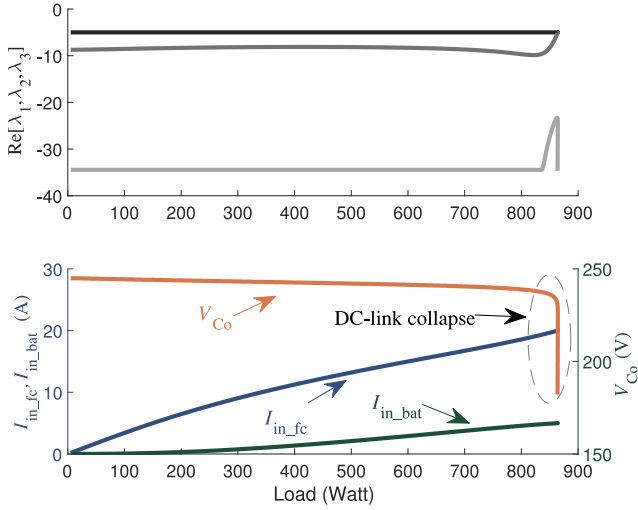


Fig. 6. Three dominant eigenvalues, fuel cell and battery currents and dc-link voltage at steady state for the load varying from 5.2 to 863.8 W with k_s according to Fig. 5.

A. Microgrid Stability

To apply the Lyapunov's Indirect Method, the first step to find the microgrid eigenvalues consists of finding the equilibrium point of (15). Then, the model is shifted to this point and the linearization is applied to find the eigenvalues that are associated with the stability around the equilibrium point. Using this approach, Fig. 6 presents the real part of the three dominant eigenvalues ($\text{Re}[\lambda_1, \lambda_2, \lambda_3]$) of (15) for loads varying from 5.2 to 863.8 W. This figure also presents the steady-state values in the equilibrium points for the sources' currents (i_{in_fc} , i_{in_bat}) and dc-link voltage (v_{Co}).

Since the k -sharing was designed, as presented in Fig. 4, as the load increases, the steady-state values of both currents (i_{in_fc} , i_{in_bat}) increase. Around 863 W of load, the fuel cell and battery currents are limited to 20 and 5 A, respectively; therefore, further increase of load leads to a dc-link collapse. Moreover, it is important to notice that the real part of the dominant eigenvalues in Fig. 6 are negative, for the tested range of load. Consequently, the microgrid is exponentially stable for the tested range of load.

B. Experimental Results

The experimental results presented in this section are compared with the simulations using the solver ode23tb with the dc microgrid model (15). It is important to highlight that the experimental results were obtained using the set of linear equations represented by the continuous lines illustrated in Fig. 5, while the simulations were obtained using the same model used for the stability analysis, i.e., they were performed using the sigmoid approximations represented by the dashed lines in Fig. 5.

In Fig. 7, the experimental results are represented by the continuous line, while the simulations using ode23tb are shown in dashed lines. An additional plot concerning the model accuracy was included in Fig. 7. In this case, the accuracy is measured using the Normalized Absolute Error in p.u., which is

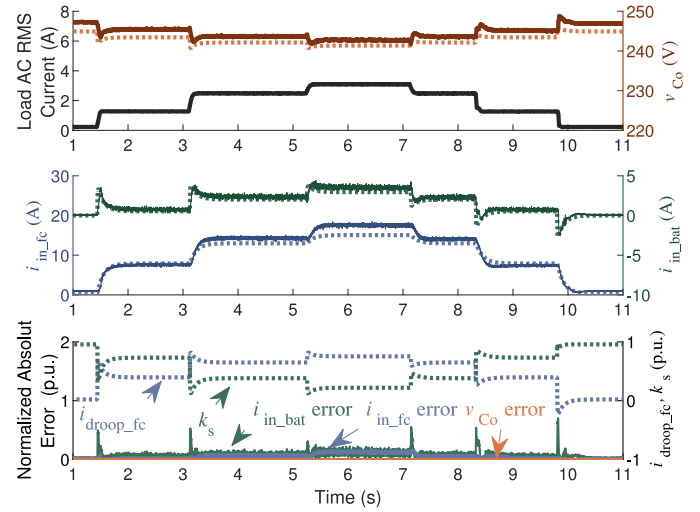


Fig. 7. Experimental results (continuous line) and simulation results (dashed line) using the model (15) with k_s according to Fig. 5 and the normalized absolute error between the experimental and simulation results.

the absolute value of the difference between the simulation and experimental result divided by the rated value. The rated values for i_{in_fc} , i_{in_bat} and v_{Co} are defined as $I_{fc_max} = 20.00$ A, $I_{bat_max} = 5.00$ A, and $V_{o_fc_0} = 245$ V, respectively.

Still in Fig. 7, since the k -sharing function was designed according to Fig. 5, the battery shares the power injected in the dc-link at the steady state and absorbs the fast transients of current. In this test, the load demand changes using the following steps of load: 252.6, 490.0, and 610.0 W. For these three different values of load, the steady-state dc-link voltage are 243.4, 242.1, and 241.4 V, respectively. As the load power increases, the fuel cell steady-state current increases, presenting the following values: 7.2, 14.45, and 17.66 A, respectively.

In this result, the battery presents a different behavior, when the load is connected; first, the battery absorbs the fast transient with a peak of current, after the transient, the current decreases to an intermediate value at the steady state. In the first load connection, the battery current i_{in_bat} achieves a peak of 3.53 A, and 0.8 A at the steady state. In the next two load connections, the current peak is 3.8 and 4.1 A, while the steady-state value for both cases are 2.5 and 3.5 A, respectively. Since the loads were connected and disconnected symmetrically, the steady-state values are the same during the load increase and decrease. In contrast, the battery current peak during the transients are different when compared with the load increase. Then, the battery current peaks for the experimental results from the beginning of load disconnection to the end of the experiment are 1.6, -0.5 , and -2.5 A, respectively.

Regarding the model accuracy, in Fig. 7, it is possible to notice that the normalized absolute error of the battery present spikes during the transients. This behavior is associated mainly with the mismatch between the model and experimental setup regarding the signal conditioning systems (hardware and software). In the experimental setup, the signal conditioning systems (hardware and software) filters the higher frequencies. However, their

dynamic response are not considered in the microgrid dynamic model (15).

According to Fig. 7, the battery and fuel cell currents also present a small steady-state error (below 0.1 p.u.), which is associated with three causes. The first cause is related with the approximation of the droop and k -sharing curves by a sigmoid function. The second is associated with the fact that the fuel cell polarization curve was not implemented in the simulation model (15). The third cause is regarding the fact that the fuel cell polarization curve changes according to, among other physical variables, the membrane's humidity [22]. Therefore, when a step of load is applied, if the membranes are not properly wet, the terminal voltage decreases very fast. For the H-1000, the system is programmed to shut down if the fuel cell terminal voltage decreases below 24 V.

In summary, the following aspects of the experimental and simulation results are associated with the main advantages of the proposed control algorithm. In every step of load, the battery responds quickly absorbing the fast current transients, while the fuel cell responds slowly until the steady-state equilibrium is achieved. Additionally, the proposed droop k -sharing function allows the battery to share the power injected in the dc-link at the steady state. With the droop k -sharing function, these features are implemented without the need of a fast link of communication between the sources.

Moreover, the small error between the simulation using the model (15) and the experimental results validate this model, and consequently, the stability analysis performed in Section VI-A.

VII. CONCLUSION

This article presented a droop k -sharing function concept, which can be used with droop controllers to fully uncouple the control loops for hybrid systems with fuel cells and storage devices, such as batteries. With this algorithm, the battery can absorb the fast transients, while the fuel cell targets the steady-state regime. Additionally, the battery can share the power delivered at the steady state with the fuel cell, according to the k -sharing function value. An advantage of this control algorithm is that the k -sharing function can be designed similarly to the droop controller.

To perform the stability analysis using Lyapunov's Indirect Method, the dc-dc converters closed-loop average model were coupled using the dc-link capacitor differential equation. Since the real part of the dominant eigenvalues are negative for the analyzed range of load, the microgrid can be considered exponentially stable in the designed operating range of load.

Finally, the effectiveness of the proposed control algorithm and the dc microgrid modeling approach for the stability analysis has been proven by comparing the microgrid model simulation results using the solver ode23tb implemented in a MATLAB script with the experimental results.

APPENDIX A

DC-DC CONVERTER AVERAGE MODEL

In this article, two different structures of dc-dc converters are used. Both structures have two transistors; however, the

modulation scheme used in these structures are different. In the buck-boost bidirectional converter, the transistors are switched using a synchronous modulation, while in the IBVM converter the transistors are switched with a 180° of displacement. Even though both structures have two transistors, only one duty-cycle (k) is applied to them.

The average modeling consists of manipulating the state-space matrices model of each switching state (16) pondered by the duty-cycle associate with each switching state.

$$\begin{cases} \dot{x} = A_1x + B_1u \\ y = C_1x + D_1u \end{cases}, \begin{cases} \dot{x} = A_2x + B_2u \\ y = C_2x + D_2u \end{cases}, \dots \quad (16)$$

Therefore, generically, the average model for dc-dc converters with only one duty-cycle results in one part dependent of the duty-cycle (A_k) and another part that is not (A_0). Finally, the matrices of the average state-space model for dc-dc converters with on duty-cycle are defined by the following:

$$\begin{cases} A = A_kk + A_0, B = B_kk + B_0 \\ C = C_kk + C_0, D = D_kk + D_0 \end{cases} \quad (17)$$

REFERENCES

- [1] O. Madani, A. Bhattacharjee, and T. Das, "Decentralized power management in a hybrid fuel cell ultracapacitor system," *IEEE Trans. Control Syst. Technol.*, vol. 24, no. 3, pp. 765–778, May 2016.
- [2] P. Thounthong, S. Rael, and B. Davat, "Control strategy of fuel cell and supercapacitors association for a distributed generation system," *IEEE Trans. Ind. Electron.*, vol. 54, no. 6, pp. 3225–3233, Dec. 2007.
- [3] M. Hamzeh, A. Ghazanfari, H. Mokhtari, and H. Karimi, "Integrating hybrid power source into an islanded MV microgrid using CHB multilevel inverter under unbalanced and nonlinear load conditions," *IEEE Trans. Energy Convers.*, vol. 28, no. 3, pp. 643–651, Sep. 2013.
- [4] C. R. de Aguiar, G. H. F. Fuzato, R. Q. Machado, and J. M. Guerrero, "An adaptive power sharing control for management of DC microgrids powered by fuel cell and storage system," *IEEE Trans. Ind. Electron.*, vol. 67, no. 5, pp. 3726–3735, May 2020.
- [5] R. T. Amin, A. S. Bambang, C. J. Rohman, R. D. Ortega, and A. Sasongko, "Energy management of fuel cell/battery/supercapacitor hybrid power sources using model predictive control," *IEEE Trans. Ind. Informat.*, vol. 10, no. 4, pp. 1992–2002, Nov. 2014.
- [6] J. Sun and I. V. Kolmanovskiy, "Load governor for fuel cell oxygen starvation protection: A robust nonlinear reference governor approach," *IEEE Trans. Control Syst. Technol.*, vol. 13, no. 6, pp. 911–920, Nov. 2005.
- [7] W. Yang, B. Bates, N. Fletcher, and R. Pow, "Control challenges and methodologies in fuel cell vehicle development," in *Proc. Int. Congr. Transp. Electron.*, vol. 2, p. 10, 1998.
- [8] S. Luo, Z. Ye, R.-L. Lin, and F. C. Lee, "A classification and evaluation of paralleling methods for power supply modules," in *Proc. 30th Annu. IEEE Power Electron. Specialists Conf. Rec.*, Jul. 1999, vol. 2, pp. 901–908.
- [9] A. P. N. Tahim, D. J. Pagano, E. Lenz, and V. Stramosk, "Modeling and stability analysis of islanded DC microgrids under droop control," *IEEE Trans. Power Electron.*, vol. 30, no. 8, pp. 4597–4607, Aug. 2015.
- [10] N. L. Diaz, T. Dragičević, J. C. Vasquez, and J. M. Guerrero, "Intelligent distributed generation and storage units for DC microgrids—A new concept on cooperative control without communications beyond droop control," *IEEE Trans. Smart Grid*, vol. 5, no. 5, pp. 2476–2485, Sep. 2014.
- [11] H. Behjati, A. Davoudi, and F. Lewis, "Modular DC-DC converters on graphs: Cooperative control," *IEEE Trans. Power Electron.*, vol. 29, no. 12, pp. 6725–6741, Dec. 2014.
- [12] T. Caldognetto and P. Tenti, "Microgrids operation based on master-slave cooperative control," *IEEE Trans. Emerg. Sel. Topics Power Electron.*, vol. 2, no. 4, pp. 1081–1088, Dec. 2014.
- [13] J. Shi, L. Zhou, and X. He, "Common-duty-ratio control of input-parallel output-parallel (IPOP) connected DC-DC converter modules with automatic sharing of currents," *IEEE Trans. Power Electron.*, vol. 27, no. 7, pp. 3277–3291, Jul. 2012.

- [14] H. Bae, J. Lee, J. Yang, and B. H. Cho, "Digital resistive current (DRC) control for the parallel interleaved DC-DC converters," *IEEE Trans. Power Electron.*, vol. 23, no. 5, pp. 2465–2476, Sep. 2008.
- [15] L. Qu, D. Zhang, and B. Zhang, "Input voltage sharing control scheme for input series and output parallel connected DC-DC converters based on peak current control," *IEEE Trans. Ind. Electron.*, vol. 66, no. 1, pp. 429–439, Jan. 2019.
- [16] L. Yifei, W. Yubin, and W. Shanshan, "Sensorless current sharing in two-phase input-parallel output-parallel DC-DC converters," in *Proc. 18th Int. Conf. Elect. Mach. Syst.*, 2015, pp. 1919–1924.
- [17] D. Sha, Z. Guo, and X. Liao, "Cross-feedback output-current-sharing control for input-series-output-parallel modular DC-DC converters," *IEEE Trans. Power Electron.*, vol. 25, no. 11, pp. 2762–2771, Nov. 2010.
- [18] J. Haubrock, G. Heideck, and Z. Styczynski, "Dynamic investigation on proton exchange membrane fuel cell systems," in *Proc. IEEE Power Eng. Soc. Gen. Meeting*, Jun. 2007, pp. 1–6.
- [19] G. H. F. Fuzato, C. R. Aguiar, K. d. A. Ottoboni, R. F. Bastos, and R. Q. Machado, "Voltage gain analysis of the interleaved boost with voltage multiplier converter used as electronic interface for fuel cells systems," *IET Power Electron.*, vol. 9, no. 9, pp. 1842–1851, 2016.
- [20] C. R. de Aguiar, G. H. F. Fuzato, R. F. Q. Magossi, R. V. A. Neves, and R. Q. Machado, "A new method to manage the fuel cell initialization," *IEEE Trans. Ind. Appl.*, vol. 54, no. 5, pp. 5187–5195, Sep. 2018.
- [21] G. H. F. Fuzato, C. R. Aguiar, R. F. Bastos, and R. Q. Machado, "Evaluation of an interleaved boost converter powered by fuel cells and connected to the grid via voltage source inverter," *IET Power Electron.*, vol. 11, no. 10, pp. 1661–1672, 2018.
- [22] K. R. de Aguiar *et al.*, "Hybrid speek/phosphonatedsilsesquioxanes membranes for PEMFC," *Nanomater. Energy*, vol. 1, no. 2, pp. 67–76, 2012.



Guilherme Henrique Favaro Fuzato (Member, IEEE) was born in Varginha, Brazil, in 1989. He received the B.S. degree in electrical engineering, the M.S. degree in power electronics and dynamic systems, and the Ph.D. degree in microgrids from the University of São Paulo, São Carlos, Brazil, in 2011, 2015, and 2019, respectively.

From 2018 to 2019, he was a Visiting Researcher with the University of Aalborg, Aalborg, Denmark. From 2012 to 2013, he was with Siemens as a Field Service Engineer in the automation area. From 2014 to 2015, he worked with Bosch with power electronics in automotive applications as a temporary Researcher. Since 2016, he has been a Lecturer with the Federal Institute of Education, Science, and Technology of São Paulo, São Paulo, Brazil. His main research interests include the fields of microgrids, energy management, and dc–dc converter for renewable energy sources and storage systems.



Cassius Rossi de Aguiar was born in Santa Maria, Brazil. He received the bachelor's degree in electrical engineering from the Federal University of Santa Maria, Santa Maria, Brazil, in 2008, and the master's and Ph.D. degrees in electrical engineering from the University of São Paulo, São Carlos, Brazil, in 2013 and 2016, respectively.

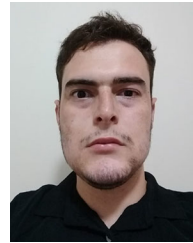
He is currently a Professor with the Federal University of Technology—Paraná, Toledo, Brazil. His main research interests include microgrids, energy management, and dc–dc converters for renewable and

storage systems.



Thales Augusto Fagundes was born in Jundiaí, Brazil, in 1992. He received the B.S. degree in electrical engineering and the M.S. degree from the University of São Paulo, São Carlos, Brazil, in 2017 and 2020, respectively. He is currently working toward the Ph.D. degree in electrical engineering with the University of São Paulo.

His main research interests include the fields of microgrids, energy management and dc–dc converters for renewable energy sources and storage systems.



Wagner Coelho Leal was born in Caratinga, Minas Gerais, Brazil. He received the B.S. degree from the Federal University of Ouro Preto, Ouro Preto, Brazil, in 2018, and the M.S. degree from University of São Paulo, São Carlos, Brazil, in 2020, both in electrical engineering.

He is currently a Researcher in Sustainable Energy with the CERTI Foundation, Florianópolis, Brazil. His research interests include analysis, control, and design of power electronic devices applied to electrical machines, electrical vehicles, distributed generation systems, and renewable energy sources.



Juan C. Vasquez (Senior Member, IEEE) received the B.S. degree in electronics engineering from the UAM, Manizales, Colombia, in 2004, and the Ph.D. degree in automatic control, robotics, and computer vision from BarcelonaTech-UPC, Barcelona, Spain, in 2009.

In 2019, he became a Professor of energy Internet and microgrids. He is currently the Co-Director of the Villum Center for Research on Microgrids, Aalborg University, Aalborg, Denmark. He was a Visiting Scholar with the Center of Power Electronics Systems (CPES), Virginia Tech, USA, and a Visiting Professor with Ritsumeikan University, Japan. His current research interests include operation, cooperative control, optimization and energy management applied to microgrids and the integration of Internet of Things and Energy Internet into the SmartGrid. He has authored and coauthored more than 460 journal papers in the field of microgrids, which in total are cited more than 19,500 times.

Prof. Vasquez has been awarded as Highly Cited Researcher by Thomson Reuters since 2017. He was the recipient of the Young Investigator Award 2019.



Josep M. Guerrero (Fellow, IEEE) received the B.S. degree in telecommunications engineering, the M.S. degree in electronics engineering, and the Ph.D. degree in power electronics from the Technical University of Catalonia, Barcelona, Spain, in 1997, 2000, and 2003, respectively.

Since 2011, he has been a Full Professor with the Department of Energy Technology, Aalborg University, Aalborg, Denmark, where he is responsible for the Microgrid Research Program. From 2019, he became a Villum Investigator by The Villum Fonden, which supports the Center for Research on Microgrids (CROM), Aalborg University, being the founder and Director of the same center. His research interests orient to different microgrid frameworks in applications like microgrid clusters, IoT-based and digital twin maritime microgrids for electrical ships, vessels, ferries and seaports, and space microgrids applied to nanosatellites and closed ecological systems. He has authored and coauthored more than 600 journal papers in the fields of microgrids and renewable energy systems, which are cited more than 50,000 times.

Prof. Guerrero was awarded by Clarivate Analytics (former Thomson Reuters) as Highly Cited Researcher with 50 highly cited papers during seven consecutive years, from 2014 to 2020. He is an Associate Editor for a number of IEEE transactions.



Ricardo Quadros Machado (Senior Member, IEEE) was born in Santa Maria, Brazil. He received the B.S. degree from the University of Santa Maria, Santa Maria, Brazil, in 1997, the M.S. and the Ph.D. degrees in electrical engineering from the University of Campinas, Campinas, Brazil, 2000 and 2005, respectively.

From 2002 to 2003, he was a visiting Researcher with the University of Padova, Padova, Italy, and from 2005 to 2007, he was a Postdoctorate with the Federal University of Santa Maria, Santa Maria, Brazil. From 2013 to 2014, he was Visiting Professor with the University of Toronto, Toronto, ON, Canada. Additionally, from 2007 to 2018, he was an Assistant Professor with the University of São Paulo, São Carlos, Brazil, where he is currently an Associate Professor. His main research interests include processing of energy in dc/dc and dc/ac converters, digital control of power converters, distributed generation systems, smart grids, and control of renewable energy sources.